New method for detecting singularities in experimental incompressible flows

Denis Kuzzay, Ewe-Wei Saw, Fabio J.W.A. Martins, Davide Faranda, Jean-Marc Foucaut, Francois Daviaud, Berengere Dubrulle

New method for detecting singularities in experimental incompressible flows

Denis Kuzzay,[1,*] Ewe-Wei Saw,[1,†] Fabio J. W. A. Martins,[2] Davide Faranda,[3] Jean-Marc Foucaut,[2] F. Daviaud,[1] and Bérengère Dubrulle[1]

[1] *SPEC, CEA, CNRS, Université Paris-Saclay, CEA Saclay, 91191 Gif-sur-Yvette, France*
[2] *Laboratoire de Mécanique de Lille, France*
[3] *Laboratoire des Sciences du Climat et de l'Environnement, LSCE/IPSL, CEA-CNRS-UVSQ, Université Paris-Saclay, F-91191 Gif-sur-Yvette, France*

We introduce two new criteria based on the work of Duchon and Robert [J. Duchon and R. Robert, Nonlinearity, 13, 249 (2000)], and Eyink [G.L. Eyink, Phys. Rev. E, 74 (2006)] which allow for the local detection of Navier-Stokes singularities in experimental flows. These criteria allow to detect areas in a flow where the velocity field is no more regular than Hölder continuous with some Hölder exponent $h \leqslant 1/2$. We illustrate our discussion using classical tomographic particle image velocimetry (TPIV) measurements obtained inside a high Reynolds number flow generated in the boundary layer of a wind tunnel. Our study shows that in order to detect singularities, one does not need to have access to the whole velocity field inside a volume, but can instead look for them from stereoscopic PIV data on a plane. We also provide a discussion making the link with the Beale-Kato-Majda criterion [J.T. Beale, T. Kato, A. Majda, Commun. Math. Phys., 94, 61 (1984)] based on the blow-up of vorticity. We show that all the criteria we study are well correlated with each other.

I. INTRODUCTION

Viscous incompressible fluids are described by the incompressible Navier-Stokes equations (INSE) in spacetime

$$\partial_t u_i + u_j \partial_j u_i = -\frac{1}{\rho}\partial_i p + \nu \partial_j \partial_j u_i + f_i \tag{1}$$

$$\partial_j u_j = 0, \tag{2}$$

where Einstein summation convention over repeated indices is used. $u_i(x,y,z,t)$ is the velocity field, $p(x,y,z,t)$ the pressure field, $\rho(x,y,z,t)$ the mass density, $f_i(x,y,z,t)$ some forcing and ν the molecular viscosity. A natural control parameter for the INSE is the Reynolds number $Re = LU/\nu$, which measures the relative importance of nonlinear effects compared to the viscous ones, and is built using a characteristic length L and velocity U. The INSE are the corner stone of many physical or engineering sciences, such as astrophysics, geophysics, aeronautics and are routinely used in numerical simulations.

However, from a mathematical point of view, it is not known whether the mechanism which tends to smooth out possible irregularities in the velocity field, i.e. viscous forces, is efficient enough to constrain u_i to remain smooth at all times. In two dimensions, the existence, unicity and smoothness theorems have been known for a long time [1–4]. In three dimensions however, it is still unclear whether the INSE are a well-posed problem, i.e. whether their solutions remain regular or develop finite time, small scale singularities. This motivated their inclusion in the AMS Millennium Clay Prize list [5]. Historically, the search for singularities in the INSE was initiated by Leray [6–8] who introduced the notion of weak solutions (i.e. in the sense of distribution). This notion has since remained a framework of choice for those wishing to study their regularity. However, only partial regularity theorems have been obtained up to now. For instance, we know that contrary to Euler equations, regularity of the solutions to the INSE is ensured if the velocity field remains bounded [9–11]. Therefore, the problem of Navier-Stokes regularity is a velocity blow-up problem, and may experimentally result in a break-down of the incompressibility condition (2) [12–14]. Another well-known result about these potential singularities, is that they are very rare events: according to the Caffarelli-Kohn-Nirenberg theorem [15] the singular set has zero one-dimensional Hausdorff measure in spacetime. This means that if they exist, singularities manifest themselves by a velocity which becomes arbitrarily large at one point in space, reaches infinity and immediately after becomes finite again.

*Electronic address: denis.kuzzay@cea.fr
†Electronic address: ewe-wei.saw@cea.fr

In 1949, Onsager published his only paper [16, 17] in the field of turbulence. In this work, he realized that far from simply being a mathematical curiosity, the possible loss of smoothness in the velocity field could have important practical consequences. More precisely, he argued that if, at point $\boldsymbol{x}$, the velocity field cannot satisfy any regularity condition stronger than a Hölder condition

$$|\boldsymbol{u}(\boldsymbol{x}+\boldsymbol{r})-\boldsymbol{u}(\boldsymbol{x})| < Cr^h, \tag{3}$$

with $h \leqslant 1/3$, then energy conservation is not ensured in the limit $\nu \to 0$ because there might exist an additional energy dissipation due to this lack of smoothness, and which has nothing to do with viscosity. Let us note that Hölder continuity (3) is a weaker regularity condition than differentiability. Therefore, at first sight, it seems that Onsager's assertion concerns the blow-up of the gradient of $\boldsymbol{u}$. However, since Navier-Stokes singularities are velocity blow-ups Onsager's statement truly is about the blow-up of $\boldsymbol{u}$ itself.
Onsager's arguments are important for turbulence because they provide an alternative mechanism to Taylor's [18, 19] in order to explain the fact that turbulent flows dissipate energy at a rate which is independent of Re, for sufficiently large Re. In the following years, Onsager's conjecture attracted a lot of attention from mathematicians, who tried to prove that $h > 1/3$ indeed imply that energy dissipation is zero when viscosity vanishes. In 2000, Duchon and Robert derived the corresponding local energy balance in Leray's weak formalism, and were in addition able to express Onsager's dissipation in terms of velocity increments [20]. Later, Eyink used the same formalism to prove that singularities may also produce a non-zero rate of velocity circulation decay, providing another interesting signature of singularities in terms of cascade of circulation [21–23].

These physical consequences illustrate the interest of detecting potential singularities of the INSE in order to advance our understanding of turbulence. This task is, however, complicated by the scarcity of the putative singularities. For example, numerical detection of singularities requires solving of the full INSE at large Reynolds numbers, for a time long enough so that singularities might develop. These two constraints actually severely limit the quest for singularities and explain why there still is no final answer about numerical detection of singularities in INSE. Part of the numerical limitations are relaxed when performing experiments with turbulent flows. Indeed, in a well-designed experiment, one can reach fairly easily large Reynolds numbers and monitor the results for a time long enough (minutes to hours) to accumulate enough statistics for reliable data analysis. In the past, experimental detection of singularities of INSE has been limited by the instrumentation, since only global (torque), or localized in space (Pitot, hot wire) or in time (slow imaging) velocimetry measurements were available. With the advent of modern particle image velocimetry (PIV), measurements of the velocity field at several points at the same time over the decimetric to sub-millimetric size range is now available, at frequencies from 1Hz to 1kHz, reviving the interest in experimental detection of singularities of INSE. The main challenge remains to find an appropriate detection method.

Clearly, the naive method consisting in tracking the velocity field and locate areas where the velocity becomes very large is unlikely to prove successful: it would require time and space resolved measurements, localized at the place where the singularity appears. With the present technology, this means zooming over a small area of the flow (typically a few mm^2) and wait until a singularity appears. Since singularities are potentially very scarce, there is little chance that one will be able to detect one. Moreover, if the velocity is indeed very high at this location, any neutral particle in the area will move very fast and leave the observation window in an arbitrarily small time. This is a problem for PIV or particle tracking velocimetry (PTV) measurements, which are based on particle tracking. An interesting alternative is provided by multifractal analysis, which is a classical but powerful method to detect singularities based on statistical multiscale analysis. Classical reviews on the method are provided in [24, 25]. With velocity fields as input, the so-called multifractal spectrum can be obtained, quantifying the probability of observation of a singularity of scaling exponent h through the fractal dimension of its supporting set $D(h)$. This method has been applied to experimental measurements of one velocity component at a single point at high Reynolds numbers in [24], where it was shown that the data are compatible with the multifractal picture, with a most probable h close to 1/3. Later Kestener and Arneodo [25] extended the method to 3D signals (3 components of the velocity field), and showed on a numerical simulation that the picture provided by the 1D measurements was still valid, with the most probable h shifting closer to 1/3. To our knowledge, this method has never been applied to 3D experimental data. Moreover, due to the statistical nature of the analysis, it appears difficult to obtain information regarding the possible instantaneous spatial distribution of singularities.

In the present paper, we suggest a new method to detect singularities inside experimental turbulent incompressible flows. This method is inspired from Onsager's conjecture and based directly on the energy balance derived by Duchon-Robert (DR) [20] (Sec. II A). The idea is to track singularities through scales by detecting the energy transfers that they produce. We will use DR's results [20] as a criterion (hereafter referred to as DR criterion) which will tell us where

to look (Sec. III). This criterion is easily implementable from now classical velocity measurements such as tomographic PIV (TPIV) or stereoscopic PIV (SPIV). Furthermore, we show that our approach provides a natural connection with the traditional cascade picture of turbulence, facilitating the interpretation of the detected singularities. We further discuss how the DR criterion compares with areas of intense vorticity (Sec III D). Finally, a result obtained by Eyink, [21–23], and which resembles Duchon and Robert's, will be investigated. This result concerns Kelvin's theorem (Sec. IV), and will give us indications on singularities with $h \leqslant 1/2$. Our discussion is illustrated using TPIV data obtained inside the boundary layer of flow generated in a wind tunnel [26].

II. MATHEMATICAL TOOLS

Lars Onsager was the first to make the connection between the regularity properties of the velocity field and kinetic energy conservation in Euler equations [16, 17, 23]. He conjectured that weak solutions of the Euler equations which are Hölder continuous with an exponent $h > 1/3$ conserve kinetic energy while those with $h \leqslant 1/3$ might not. Since then, efforts were made in order to prove this assertion [27, 28]. A milestone was reached with the work of Duchon and Robert [20], who derived the exact local form of the energy dissipation created by a loss of regularity in the velocity field, along with the corresponding energy balance. In this section, we provide the basic mathematical tools in order to understand these ideas.

A. Background on Onsager's conjecture

A physical way of discussing Onsager's conjecture is to consider a local space averaged (low-pass filtered) velocity field. In the INSE, the unknown velocity and pressure fields contain informations about the flow at all possible scales. Let us define a coarse-grained velocity field by taking the convolution of $\boldsymbol{u}$ with some kernel G_ℓ

$$u_i^\ell(\boldsymbol{x},t) = \int d\boldsymbol{r}\; G_\ell(\boldsymbol{r})\, u_i(\boldsymbol{x}+\boldsymbol{r},t)\,, \tag{4}$$

where G is a smooth filtering function with compact support on $\mathbb{R}^3$, even, non-negative, spatially localized and such that $\int d\boldsymbol{r}\; G(\boldsymbol{r}) = 1$. The function G_ℓ is rescaled with ℓ as $G_\ell(\boldsymbol{r}) = \ell^{-3} G(\boldsymbol{r}/\ell)$. This process of coarse-graining thus averages out fine details about the fields while keeping informations about large scales. Formally, the coarse-grained velocity can be seen as a continuous wavelet transform of the velocity $\mathbf{u}$ with respect to the wavelet G. Note, however, that since we have chosen G to be of unit integral, it is not admissible, meaning that the wavelet transform is not invertible. Let us now derive the equations satisfied by u_i^ℓ. Starting from the INSE and applying the coarse-graining procedure we get

$$\partial_t u_i^\ell + u_j^\ell \partial_j u_i^\ell = f_i^\ell - \partial_i p^\ell + \nu \partial_{jj} u_i^\ell, \tag{5}$$

$$\partial_j u_j^\ell = 0, \tag{6}$$

where $f_i^\ell = -\partial_j \tau_{ij}^\ell$ is called the turbulent force, and $\tau_{ij}^\ell = (u_i u_j)^\ell - u_i^\ell u_j^\ell$ is the subscale stress tensor. We thus obtain a sequence of equations describing the dynamics of large scales. From these equations, together with the INSE (1) and (2), we can derive a local energy balance at scale ℓ

$$\partial_t E^\ell + \partial_j J_j^\ell = -\Pi_{DR}^\ell - \mathscr{D}_\nu^\ell, \tag{7}$$

where each term in Eq. (7) take the form [20, 29]

$$E^\ell = \frac{u_i u_i^\ell}{2}, \tag{8}$$

$$J_j^\ell = u_j E^\ell + \frac{1}{2}\left(p u_j^\ell + p^\ell u_j\right) + \frac{1}{4}\left[(u_i u_i u_j)^\ell - (u_i u_i)^\ell u_j\right] - \nu \partial_j E^\ell + \nu \int \nabla_i G_\ell(\xi) u_j(x) u_j(x+\xi) d\xi, \tag{9}$$

$$\Pi_{DR}^\ell = \frac{1}{4}\int d\boldsymbol{r}\; \nabla_i G_\ell(\boldsymbol{r}) \cdot \delta u_i(\boldsymbol{x},\boldsymbol{r}) |\delta \boldsymbol{u}(\boldsymbol{x},\boldsymbol{r})|^2, \tag{10}$$

$$\mathscr{D}_\nu^\ell = -\nu \int d\boldsymbol{r}\; \nabla_{jj} G_\ell(\boldsymbol{r}) u_i(\boldsymbol{x})\, u_i(\boldsymbol{x}+\boldsymbol{r})\,, \tag{11}$$

where ∇ is the derivative with respect to r and $\delta\boldsymbol{u}(\boldsymbol{x},\boldsymbol{r}) = \boldsymbol{u}(\boldsymbol{x}+\boldsymbol{r}) - \boldsymbol{u}(\boldsymbol{x})$. In Eq. (7), E^ℓ represents the large-scale kinetic energy, J_j^ℓ is the large-scale energy current in space, Π_{DR}^ℓ describes the local amount of energy scattered through scale ℓ (see [30] for an application to experimental measurements), and $\mathscr{D}_\nu^\ell$ is the viscous energy dissipation at scale ℓ.
Taking the limit of infinitely small scales $\ell \to 0$, we obtain the local energy balance

$$\partial_t E + \partial_j J_j = -\mathscr{D}_I - \mathscr{D}_\nu, \tag{12}$$

where all the derivatives should be understood in the weak sense, i.e. in the sense of distributions. Moreover, the various terms of Eq. (12) take the form

$$E = \frac{u_i u_i}{2}, \tag{13}$$

$$J_j = u_j\,(E+p) - \nu\partial_j E, \tag{14}$$

$$\mathscr{D}_I = \lim_{\ell\to 0}\ \frac{1}{4}\int d\boldsymbol{r}\ \nabla_i G_\ell(\boldsymbol{r})\cdot\delta u_i(\boldsymbol{x},\boldsymbol{r})|\delta\boldsymbol{u}(\boldsymbol{x},\boldsymbol{r})|^2, \tag{15}$$

$$\mathscr{D}_\nu = \nu\partial_j u_i \partial_j u_i, \tag{16}$$

and $\mathscr{D}_I$ is called the local inertial energy dissipation. In the classical picture of turbulence, $\boldsymbol{u}$ remains smooth ($\boldsymbol{u}\in C^\infty$) for all scales so that $\delta u \sim \ell$ as $\ell \to 0$. In this case, $\mathscr{D}_I = 0$ and Eq. (12) is the usual local balance of energy. However, mathematically, it is not known whether a solution of the INSE which is smooth at some initial time remains smooth at all later times, and Onsager's key idea was to consider weaker regularity conditions on $\boldsymbol{u}$. In particular, let us consider a velocity field which is Hölder continuous with some exponent $h < 1$ (i.e. not necessarily differentiable) at small scales. We have

$$|\boldsymbol{u}(\boldsymbol{x}+\boldsymbol{r}) - \boldsymbol{u}(\boldsymbol{x})| < Cr^h, \tag{17}$$

or equivalently

$$|\delta\boldsymbol{u}(\boldsymbol{x},\boldsymbol{r})| = \underset{r\to 0}{O}\left(r^h\right). \tag{18}$$

Let us now define $\delta u(\boldsymbol{x},\ell) \overset{def}{=} \underset{r<\ell}{sup}\,|\delta\boldsymbol{u}(\boldsymbol{x},\boldsymbol{r})|$ [23]. We directly get that

$$\Pi_{DR}^\ell = \underset{\ell\to 0}{O}\left(\frac{\delta u(\boldsymbol{x},\ell)^3}{\ell}\right). \tag{19}$$

Therefore, if $\boldsymbol{u}$ is Hölder continuous in space with exponent h, i.e. $\delta u(\ell) \sim \ell^h$, then

$$\Pi_{DR}^\ell = \underset{\ell\to 0}{O}\left(\ell^{3h-1}\right). \tag{20}$$

As a consequence, we see that if $h > 1/3$, Π_{DR}^ℓ vanishes as $\ell \to 0$ and Euler equations are seen to conserve energy ($\mathscr{D}_\nu = 0$). On the other hand, it may well be that this condition does not hold, in which case turbulent flows might keep on dissipating energy even if $\nu = 0$.
All the steps we have described here have been formalized for the first time in a rigorous mathematical framework by Duchon and Robert [20]. They found the expression given in Eq. (15) for the inertial dissipation, and showed that it does not depend on the choice of the test function G. The key point of their work is that $\mathscr{D}_I$ appears in Eq. (12) as the fraction of energy dissipated due to a lack of smoothness in the velocity field, and has nothing to do with viscosity.

B. Connection with traditional turbulence notions

1. The zeroth law of turbulence

It is a well-known experimental fact that for high enough Reynolds numbers, the global dimensionless energy dissipation rate per unit mass ϵ is a nonzero constant independent of Re. This observation was first reported by Taylor [31], in a paper discussing turbulent pipe flows, and is known as the zeroth law of turbulence. Since Taylor, the zeroth law of turbulence has found many confirmations in several other experiments [32–35] and DNS [36–41] in various geometries, but a derivation from the INSE has yet to be found. The zeroth law therefore suggests that the mean energy dissipation rate of turbulent flows remains finite even after the limit $Re \to \infty$ has been taken, which constitutes one of the fundamental assumptions at the heart of Kolmogorov's theory of 1941 (K41) [42].
After his discovery of the zeroth law, Taylor proposed a physical mechanism for energy dissipation based on viscosity and Richardson's cascade picture [18, 19]. Taylor used vortex stretching to argue that by incompressibility, the stretching of vortex lines will be accompanied by a reduction of the cross section of any vortex tube in which they are contained, leading to an increase of $\boldsymbol{\omega}^2$ through Kelvin's theorem. Now, noting that the mean viscous energy dissipation can be expressed as $\overline{\mathscr{D}_\nu} = \nu\overline{\boldsymbol{\omega}^2}$ (where the overline denotes space averaging), it is easy to understand that if $\overline{\boldsymbol{\omega}^2} \sim \nu^{-1}$ at small scales, the mean dissipated power $\epsilon = \nu\overline{\boldsymbol{\omega}^2}$ becomes independent of the viscosity.
Onsager's key remark was that energy dissipation may take place just as well without the final assistance by viscosity, because Euler equations do not necessarily conserve energy if the velocity field is not regular enough. Indeed, as we argued in Sec. II A, solutions to the INSE which cannot satisfy any Hölder condition with an exponent $h > 1/3$ may produce an inertial dissipation independently of viscosity. Therefore, Onsager's scenario can be viewed as an alternative to Taylor's. An interesting point is that $h = 1/3$ in K41, which is also the maximum regularity condition compatible with a nonzero inertial dissipation.

2. Kármán-Howarth-Monin relation

A corner stone of turbulence theory is provided by the Kármán-Howarth-Monin (KHM) relation [12, 43–45], valid for homogeneous turbulence, linking the energy injection per unit mass ϵ_I and velocity increments via

$$\frac{1}{2}\partial_t\langle u_i(\boldsymbol{x})\, u_i(\boldsymbol{x}+\boldsymbol{\ell})\rangle = \frac{1}{4}\nabla_i\langle \delta u_i(\boldsymbol{\ell})\,|\delta\boldsymbol{u}(\boldsymbol{\ell})|^2\rangle + \nu\nabla_{jj}\langle u_i(\boldsymbol{x})\, u_i(\boldsymbol{x}+\boldsymbol{\ell})\rangle + \epsilon_I, \tag{21}$$

where $\langle\rangle$ denotes statistical average, and we have dropped the dependence of $\delta\boldsymbol{u}$ on $\boldsymbol{x}$ by homogeneity. In Eq. (21), $E(\ell) = \langle u_i(\boldsymbol{x})\, u_i(\boldsymbol{x}+\boldsymbol{\ell})\rangle$ is a measure of the kinetic energy at scale ℓ. It is interesting to note that taking the statistical average of Eq. (7) and integrating over space, we get the following equation

$$\frac{1}{2}\partial_t\int d\boldsymbol{\xi}\; G_\ell(\boldsymbol{\xi})\, E(\boldsymbol{\xi}) - \epsilon_I = -\frac{1}{4}\int d\boldsymbol{\xi}\; \nabla_i G_\ell(\boldsymbol{\xi})\,\langle \delta u_i(\boldsymbol{\xi})\,|\delta\boldsymbol{u}(\boldsymbol{\xi})|^2\rangle + \nu\int d\boldsymbol{\xi}\; \nabla_{jj} G_\ell(\boldsymbol{\xi})\, E(\boldsymbol{\xi}). \tag{22}$$

In order to obtain Eq. (22), we have assumed that the energy input is provided by boundary conditions. Since the global contribution of the divergence of the energy current in Eq. (7) can be reduced to the flux of J at the boundaries, we therefore get that $\int\langle\partial_j J_j\rangle = -\epsilon_I$. As a consequence, one recognizes in Eq. (22) a weak formulation of the homogeneous KHM relation, which can also be considered as the average over a sphere of radius ℓ of the KHM relation. Now if we relax the conditions on the test function G that we imposed in Sec. II A, we see that taking $G_\ell = \exp(i\boldsymbol{k}\cdot\boldsymbol{x})$ with $\boldsymbol{k} = \boldsymbol{\ell}/\ell^2$ in Eq. (22) leads to the classical energy budget in Fourier space, where $\int\langle E^\ell\rangle = E(\boldsymbol{k})$ is the energy density at wavenumber $\boldsymbol{k}$, $\int\langle\mathscr{D}_\nu^\ell\rangle = \nu\boldsymbol{k}^2 E(\boldsymbol{k})$ is the viscous energy dissipation, and $\int\langle\Pi_{DR}^\ell\rangle = \Pi(\boldsymbol{k})$ is the scale-to-scale energy transfer rate.
Π_{DR}^ℓ therefore appears in Eq. (7) as a local expression of the scale-to-scale energy transfer of the KHM relation which is valid even when the flow is anisotropic, inhomogeneous, and when $\boldsymbol{u}$ is not differentiable. This constitutes the main difference with its counterpart in Eq. (21). However, it was shown in [20] that assuming homogeneity, both terms have the same small-scale limit. Eq. (7) can then be viewed as a generalization of Eq. (21) to inhomogeneous flows, therefore making the link with Onsager's conjecture.

3. Practical implementation and Noise issues

The practical applicability of the KHM relation to turbulence relies on the fact that the statistical average of the third order structure function $\langle \delta \boldsymbol{u} | \delta \boldsymbol{u}|^2 \rangle$ is smooth enough to be differentiable. This is often the case if the turbulence is locally homogeneous, and if the experimental noise is isotropic, Gaussian and not correlated to the velocity measurements, as is often the case in absence of systematic errors. In such a case, the measured velocity increments can be simply written as $\delta \boldsymbol{u}_{meas} = \delta \boldsymbol{u} + \boldsymbol{\alpha}$, where $\delta \boldsymbol{u}$ is the true velocity increment and $\boldsymbol{\alpha}$ is the noise, such that for any (i,j,k) $\langle \alpha_i \rangle = \langle \alpha_i \alpha_j \alpha_k \rangle = 0$ and $\langle \alpha_i \alpha_j \rangle = \mathcal{N} \delta_{ij}$, where $\mathcal{N}$ is the noise amplitude. Since we further have

$$\delta \boldsymbol{u}_{meas} |\delta \boldsymbol{u}_{meas}|^2 = \delta \boldsymbol{u} |\delta \boldsymbol{u}|^2 + \boldsymbol{\alpha} |\delta \boldsymbol{u}|^2 + 2 \delta \boldsymbol{u} \left(\boldsymbol{\alpha} \cdot \delta \boldsymbol{u} \right) + 2 \boldsymbol{\alpha} \left(\boldsymbol{\alpha} \cdot \delta \boldsymbol{u} \right) + \delta \boldsymbol{u} |\boldsymbol{\alpha}|^2 + \delta \boldsymbol{\alpha} |\delta \boldsymbol{\alpha}|^2, \tag{23}$$

we get by statistical averaging

$$\langle \delta \boldsymbol{u}_{meas} |\delta \boldsymbol{u}_{meas}|^2 \rangle = \langle \delta \boldsymbol{u} |\delta \boldsymbol{u}|^2 \rangle + 3 \mathcal{N} \langle \delta \boldsymbol{u} \rangle. \tag{24}$$

If the velocity field is locally homogeneous then $\langle \delta \boldsymbol{u} \rangle = 0$, so that all the noise contribution has been averaged out and there is no noise amplification introduced by taking the divergence. In the same way, if the noise has no spatial correlation, the statistical average guarantees that the noise contribution is averaged out in $\langle E(\ell) \rangle$, so that it can be differentiated twice without noise amplification. This means that both the energy transfer and the dissipation term in the KHM relation can be computed with minimal noise from homogeneous, experimental fields.
The weak formulation ensures that this property is transferred in the computation of local instantaneous energy transfers via Π^ℓ_{DR} and of the dissipation term $\mathscr{D}^\ell_\nu$, in areas where the turbulence is homogenous. Indeed, the gradient is not applied directly to the velocity increments, but rather on the smooth test function, preceded by a local angle averaging. The latter plays a role similar to statistical averaging for isotropic noise. The convolution with the derivative of the smoothing function further guarantees no experimental noise amplification. There is no additional noise induced by this procedure if one recognizes that the volume integrals performed in Π^ℓ_{DR} and $\mathscr{D}^\ell_\nu$ can be simply done via either continuous wavelet transform, or direct and reverse Fast Fourier Transforms and multiplication in Fourier space by the derivative of the smoothing function, which can be computed analytically to avoid discretization effects. This robustness with respect to noise makes the quantity Π^ℓ_{DR} a very interesting tool to localize potential singularities in both space and time, as we discuss in Sec. III A. Note finally that the expression of Π^ℓ_{DR} is very suitable for its implementation from experimental particle image velocimetry (PIV) measurements: it involves only velocity increments, which are easily computed from the velocity field data obtained by such technique.

4. Euler singularities vs Navier-Stokes singularities and the multifractal model

There are evidences coming from direct numerical simulations that turbulent velocity fields admit a local scaling symmetry through the existence of a continuous set of scaling (Hölder) exponents $h(x)$, with the most probable exponent close to $1/3$ [24, 25]. These exponents can be defined as

$$h(\boldsymbol{x}) = \lim_{\ell \to 0} \frac{\ln |\delta \boldsymbol{u}(\boldsymbol{x}, \boldsymbol{\ell})|}{\ln(\ell / L)}, \tag{25}$$

where L is a characteristic integral length of scale. These points correspond to location where the scaling symmetry of the Euler equations $(t, \boldsymbol{x}, \boldsymbol{u}) \to (\lambda^{1-h} t, \lambda \boldsymbol{x}, \lambda^h \boldsymbol{u})$ is locally satisfied [12], which means that the definition in Eq. (25) is valid under the assumption that $\nu \to 0$.
It can be seen that the above definition of h has a mathematical interest only for $0 \leqslant h \leqslant 1$. However, it might be that this condition becomes too restrictive for practical purposes, in which case another definition should be come up with. As a matter of fact, there are several ways of doing so, and a discussion is provided in [46]. In particular, using wavelet coefficients, the definition of h can be extended to $h < 0$, which takes power-law blow-ups of the velocity field into account. Such blow-ups would then be identified as possible singularities of the Euler equation.
In the multifractal model of turbulence [47], it can be shown that the Hölder exponent at scale r, defined as

$$h(\boldsymbol{x}, \boldsymbol{r}) = \frac{\ln |\delta \boldsymbol{u}(\boldsymbol{x}, \boldsymbol{r})|}{\ln(r/L)}, \tag{26}$$

follows a large deviation property [46]

$$\text{Prob}\left(h\left(\boldsymbol{x},\boldsymbol{r}\right)=h\right)\sim\left(\frac{r}{L}\right)^{C(h)}, \tag{27}$$

where $C(h)$ formally corresponds to the codimension of the set where the local Hölder exponent at scale r is equal to h. Multifractal analysis of DNS or experimental data proved that the most probable exponent is $h=1/3$ with $C\left(1/3\right)\approx 0$ [24, 25].
If we now consider a flow with finite viscosity, we have seen that the local energy balance at scale ℓ is provided by Eq. (7). For a flow following locally $\delta\boldsymbol{u}\left(\boldsymbol{x},\boldsymbol{\ell}\right)\sim\ell^h$, we have $\Pi_{DR}^{\ell}\sim\ell^{3h-1}$ and $\mathscr{D}_{\nu}^{\ell}\sim\nu\ell^{2h-2}$. These two terms balance at a scale $\eta_h\sim\nu^{1/(1+h)}$. η_h thus appears as a fluctuating cut-off which depends on the scaling exponent and therefore on $\boldsymbol{x}$. This is the generalization of the Kolmogorov scale $\eta_{1/3}=(\nu^3/\epsilon)^{1/4}$, and was first proposed in [48]. As a consequence, η_h corresponds to the scale at which any possible Euler singularity of exponent h is regularized by viscosity. Above η_h, $\delta\boldsymbol{u}\left(\boldsymbol{x},\boldsymbol{\ell}\right)\sim\ell^h$ and energy is transferred towards small scales via Π_{DR}^{ℓ} until $\ell=\eta_h$ is reached and where $\Pi_{DR}^{\ell}\sim\epsilon\left(\eta_h/L\right)^{3h-1}$. Below η_h, the flow is regularized by viscous forces and $\delta\boldsymbol{u}\left(\boldsymbol{x},\boldsymbol{\ell}\right)\sim\ell$ so that Π_{DR}^{ℓ} decreases to 0 like ℓ^2, kinetic energy being dissipated into heat by viscosity. As a consequence, if $-1<h\leqslant 1/3$, Onsager's scenario can only occur in the absence of viscosity. For this reason, we call such solutions dissipative Euler quasi-singularities. A noticeable exception comes from the case $h=-1$, for which $\eta_{-1}=\lim_{h\to-1}Re^{-1/(1+h)}=0$ at sufficiently large Re. For this exponent, there is no possibility of regularization by viscosity ($1/r$ is a zero mode of the Laplacian), so that $h=-1$ might correspond to a Navier-Stokes singularity which would dissipate energy at infinitely small scales, following Onsager's scenario. This is in agreement with the work of Cafarelli et al. [15] who showed that if a singularity appears at some point in spacetime which we denote $(\boldsymbol{X}_*,T_*)$, then at $t=T_*$, $|\boldsymbol{u}|\to\infty$ at least like $|\boldsymbol{x}-\boldsymbol{X}_*|$.

The question now is: provided that such singularities actually occur, do they have a nonzero contribution to the total energy dissipation ? The answer to this question depends on the value of the codimension $C(-1)$. Indeed, the total contribution to the energy transfers for a given h scales like $\langle\Pi_{DR}^{\ell}\rangle\sim\ell^{3h-1+C(h)}$. We see that for $h=-1$, it is necessary to have $C(-1)=4$ for $\langle\Pi_{DR}^{\ell}\rangle$ to be finite as $\ell\to 0$. This is in agreement with the well-known result of Cafarelli et al. [15], who showed that the singular set of the INSE, if it exists, has zero one-dimensional Hausdorff measure. More discussions on this matter are provided in [46].

5. *Energy transfers*

In the multifractal picture, the maximum amount of energy transfers depends on the local Hölder exponent: for $1/3<h<1$, the energy transfers generally decrease as $\ell\to 0$, so that it typically never exceeds ϵ. This corresponds to non-dissipative Euler quasi-singularities. For $h<1/3$, the energy transfers increase with scale until $\ell\approx\eta_h$, so that they can reach large values $\epsilon\left(\eta_h/L\right)^{3h-1}\gg\epsilon$, even below the Kolmogorov scale $\eta=\eta_{1/3}$. Therefore, it appears possible to track possible Euler quasi-singularities or even Navier-Stokes singularities ($h=-1$), by monitoring the energy transfers at or below the Kolmogorov scale, and looking for locations where it exceeds the global energy dissipation by a large fraction. The method of detection of singularities we present in Sec. III relies on this remark. Moreover, using a steepest descent argument, it is possible to estimate at each scale the mean energy transfer due to all quasi-singularities as

$$\overline{\Pi_{DR}^{\ell}}\sim\ell^{\min_h[3h-1+C(h)]}\sim\ell^{\zeta(3)-1}, \tag{28}$$

where $\zeta(p)=\min_h\left[ph-1+C(h)\right]$ is the exponent of the p^{th} order structure function, depending on the singularity distribution through the shape of $C(h)$. In the K41 theory $\zeta(3)=1$, so that $\overline{\Pi_{DR}^{\ell}}$ is constant over the inertial range.

III. SINGULARITY DETECTION THROUGH DUCHON-ROBERT FORMULA

A. Detection method

We saw in Sec. II A that if the velocity is locally characterized by a scaling exponent $h>-1$, then the energy transfer Π_{DR}^{ℓ} locally vanishes for scales much smaller than η_h. In this section, we will make use of the converse statement

of this result, i.e. if locally at a certain scale Π^ℓ_{DR} takes very large values, then the flow in the region where this is observed is a Navier-Stokes singularity (possibly with $h = -1$) or a dissipative Euler-quasi singularity which has not been regularized yet. In the former case, the velocity field is not differentiable, which necessarily comes from a blow-up of the velocity field itself [9–11, 15]. However, there are several reasons why such singularities cannot be directly detected from experimental measurements. First of all, measurement systems inevitably have a coarse space and time resolution while blow-ups occur instantaneously at one point [15]. Furthermore, post-processing techniques which provide the output velocity field smooth the data by performing local averages, and by considering very large velocities as spurious vectors which, in the end, are discarded. The key idea is therefore to track possible singularities through the behaviour of Π^ℓ_{DR} as one comes across the dissipative scale $\eta = \eta_{1/3}$. If Π^ℓ_{DR} vanishes as one approaches or goes to smaller scales than η, then we have only seen local energy transfers through scales [30], which is ultimately converted into heat by viscous frictions, as in the traditional Taylor view of turbulence. If on the other hand, we see that Π^ℓ_{DR} keeps a nonzero value larger than some threshold $\mathcal{Q}$ for $0 < \ell < \eta$, then we have detected a structure connected to a dissipative Euler quasi-singularity or Navier-Stokes singularity. In general, we can expect that the larger the threshold $\mathcal{Q}$, the smaller the exponent h we probe. For fixed viscosity and decreasing ℓ, we may even expect that arbitrary large values of $\mathcal{Q}$ only correspond to genuine Navier-Stokes singularities.
The only adjustable parameter in our detection method is the threshold $\mathcal{Q}$. A natural choice for $\mathcal{Q}$ is to take

$$\mathcal{Q}(\ell) = Q\sigma_{DR}(\ell), \tag{29}$$

where the σ_{DR} denotes the standard deviation of Π^ℓ_{DR}. Q therefore characterizes the quantile of the distribution of quasi-singularities [49]. For example, if $Q = 10$, we select events with an amplitude 10 times larger than the expected deviation from the spacetime average of Π^ℓ_{DR}. With $Q = 100$, we select more extreme quasi-singularities, which represent in general very rare events, presumably closer to the case $h = -1$ (Navier-Stokes singularities). In extreme value theory, there is no general rule as to what quantile should be used in order to consider an event as extreme. The most common choice when the events are normally distributed is to take $Q = 3 - 5$. In the rest of the paper we use $Q = 3$.
In all our computations, we have used a spherically symmetric function of $\boldsymbol{r}$ given by

$$G(r) = \begin{cases} \frac{1}{N}\exp\left(-\frac{1}{1-r^2/4}\right) & \text{for } 0 \leqslant r \leqslant 1, \\ 0 & \text{otherwise,} \end{cases} \tag{30}$$

where N is a normalization constant such that $\int d\boldsymbol{r}\ G(r) = 1$. G has a compact support and satisfies the properties given in Sec. II A.

B. Implementation

We illustrate our detection method using experimental velocimetry measurements. The data are tomographic particle image velocimetry (TPIV) measurements performed inside a boundary layer of a wind tunnel located at the Laboratoire de Mécanique de Lille, France. A sketch of the experimental set-up is displayed in Fig. 1 along with a typical instantaneous frame in a plane orthogonal to the mean flow. The test section of the wind tunnel is 1m high, 2m wide and 20m long. The boundary layer thickness can reach up to 300mm and the Reynolds number R_θ based on the momentum thickness is $R_\theta = 8000$, with a wall region of around 40mm. The TPIV system is composed of six high-speed cameras recording the flow into a volume normal to the wall (see Fig . 1). The investigation volume is $5 \times 45 \times 45$ mm^3 and, in the end, we get the three components of the velocity field on a grid of size $5 \times 67 \times 67$. Note that for these data, the resolution (grid spacing) is $\Delta x = 0.7$mm while the Kolmogorov scale is of the order of $\eta \approx 0.35$mm. Therefore, we will be able to test the DR criterion at scales close to the dissipative scale. Let us finally make a small remark about the inertia of the particles. The wind tunnel was operated in a close-loop configuration with a free stream velocity of 3 m/s $\pm$ 0.5% and a temperature of 15 ± 0.2 °C. The whole flow was seeded with polyethylene glycol smoke, which generates particles with a size of the order of 1µm. We can therefore compute their Stokes number which is $S_t \approx 4 \times 10^{-4}$. As a consequence, we have between two and three orders of magnitudes before the inertia of the particles become appreciable. Since we have also $S_t \approx \sqrt{\epsilon}$, this will happen in regions where ϵ is at least 10^4 times larger than its average.
An example of variation of $\Pi^\ell_{DR}(\boldsymbol{u})/\sigma_{DR}$ as a function of scale ℓ and position $\boldsymbol{x}$ in a plane orthogonal to the mean flow is provided in Fig. 2. In this figure, the scale is expressed in units of the Kolmogorov scale η. For scales $\ell \gtrsim 8\eta$, the topology of the ratio $\Pi^\ell_{DR}(\boldsymbol{u})/\sigma_{DR}$ does not vary much. This range of scales represent the end of the inertial

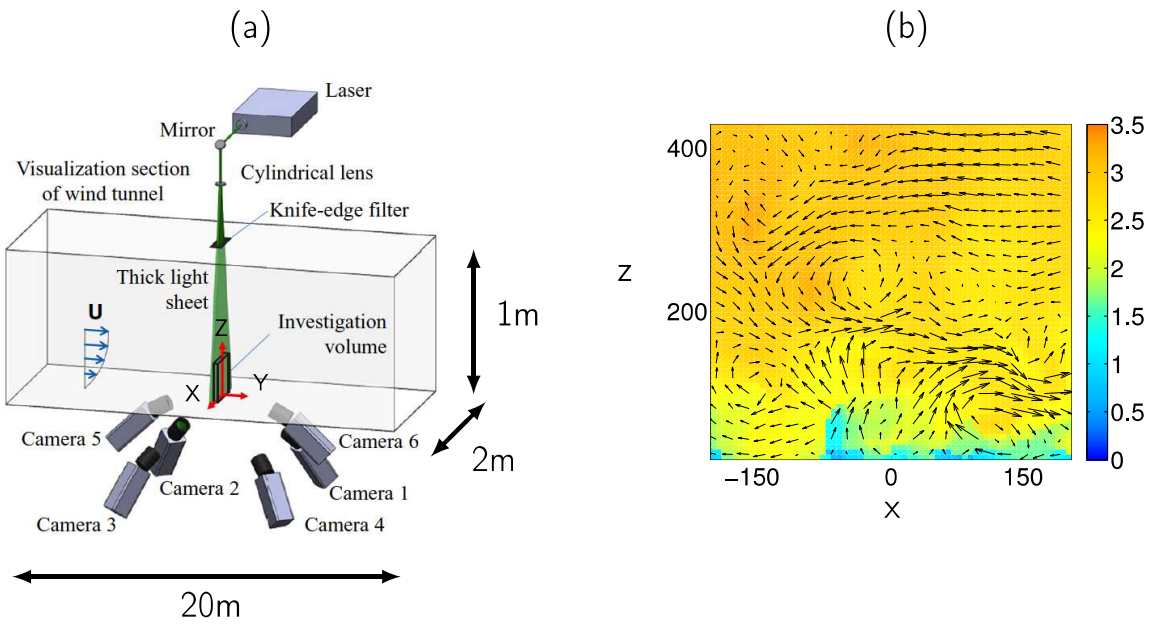

FIG. 1: (a) sketch of the experimental set-up and (b) typical instantaneous velocity field, obtained from TPIV measurements in a plane orthogonal to the mean flow. The arrows represent the in-plane component of the velocity field while the colors code the normal component.

inertial range where the Π^ℓ_{DR} captures the cascade of energy [30]. On the other hand, as we reach the dissipative range, i.e. $\ell \lesssim 8\Delta x$, $\Pi^\ell_{DR}(\boldsymbol{u})/\sigma_{DR}$ changes topology. We see that Π^ℓ_{DR} does not vanish, but instead remains larger than some threshold Q, which in several frames is found to be $Q = 10$, at localized areas which we identify as possible quasi-singularities with $h \leqslant 1/3$.

As explicitly written in Eq. (29), σ_{DR} depends on the scale ℓ. This can be seen on Fig. 3 which displays the spacetime probability distribution of Π^ℓ_{DR} in the XZ-plane studied in Fig. 2(a), in the stationary regime at three different scales (the same as in Fig. 2(a)). We observe that the statistics of Π^ℓ_{DR} is strongly non-Gaussian with very large tails [50]. It can be checked from these distributions that as ℓ is decreased, the spacetime average as well as the standard deviation of Π^ℓ_{DR} increases. As a consequence, we obtain distributions with wider tails at smaller scales, and we detect more extreme events corresponding to possible quasi-singularities. In the three cases displayed on Fig. 3, it can be seen that the distributions are slightly skewed towards positive values, which allows the spacetime average of Π^ℓ_{DR} to remain positive, in agreement with [30].

C. 2D vs 3D detection

In principle, our method of detection requires the input of the three components of the velocity field in a volume, i.e. requires data from TPIV. In practice, some PIV systems are only stereoscopic, giving access to the three components of the velocity field on a plane only, but allowing for very long statistics. Since velocity increments along one direction of space cannot be computed, this raises the question of whether the DR criterion is still able to detect quasi-singularities from SPIV data, or does the absence of the third direction lead to the detection of spurious structures which would disappear if the full 3D computation were to be performed ? To answer this question, let us define a new quantity based on the inertial dissipation $\mathscr{D}_I$, which is built from the three components of the velocity increments on a two dimensional plane

$$\mathscr{D}_I^{2D}(\boldsymbol{u}) \overset{def}{=} \lim_{\ell\to 0} \Pi^{\ell,2D}_{DR}(\boldsymbol{u}) = \lim_{\ell\to 0} \frac{1}{4}\int_{\mathcal{S}} d\boldsymbol{r}\ \partial_i G_\ell(\boldsymbol{r}) \cdot \delta^{2D} u_i(\boldsymbol{r})\ |\delta^{2D}\boldsymbol{u}(\boldsymbol{r})|^2, \tag{31}$$

where $\delta^{2D}\boldsymbol{u}(\boldsymbol{r}) = \boldsymbol{u}(\boldsymbol{x}^{2D} + \boldsymbol{r}^{2D}) - \boldsymbol{u}(\boldsymbol{x}^{2D})$, $\boldsymbol{x}^{2D}$ and $\boldsymbol{r}^{2D}$ being the projection onto the plane of measurements of the

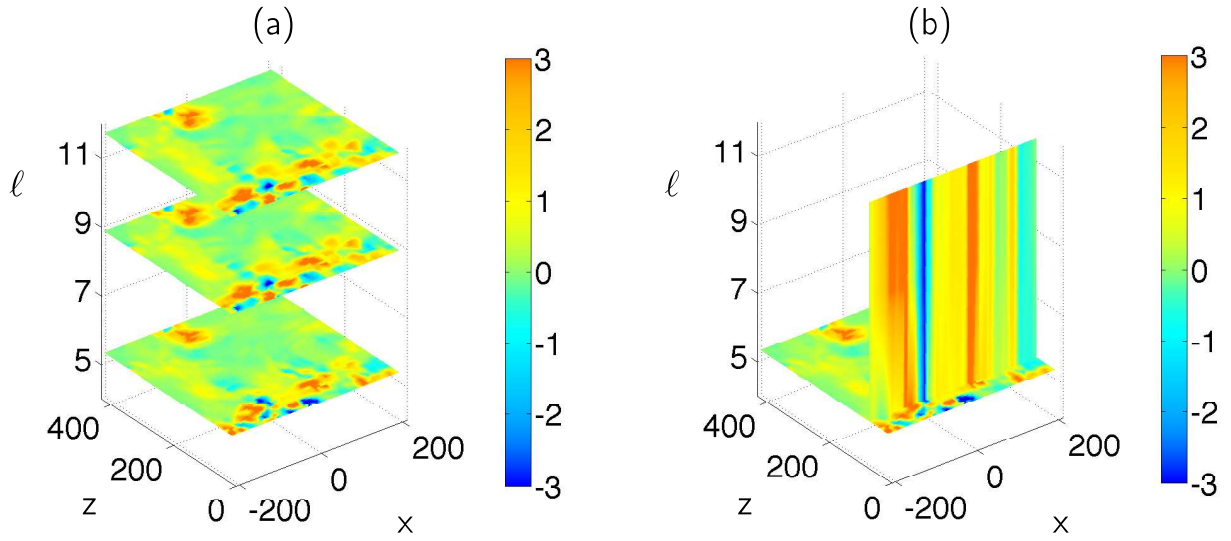

FIG. 2: Maps of the Duchon-Robert (DR) energy transfers as a function of scale ℓ. (a) map of Π^{ℓ}_{DR} at three different scales and (b) map of Π^{ℓ}_{DR} at different scales along a line going through possible quasi-singularities. In both maps, Π^{ℓ}_{DR} has been normalized by its standard deviation. The results are displayed in the plane $y = 0$ orthogonal to the streamwise direction, and the colors code $\Pi^{\ell}_{DR}(\boldsymbol{u})/\sigma_{DR}$. The scale is expressed in units of the Kolmogorov scale (0.35mm).

3D coordinates. We now argue that areas where the full field $\mathscr{D}_I(\boldsymbol{u})$ is zero are also areas where $\mathscr{D}^{2D}_I(\boldsymbol{u})$ is zero, thus proving that no spurious singularities are detected in SPIV data.
To prove this, we note $\mathcal{B}_\ell(\boldsymbol{x})$ the ensemble of all the velocity increments of maximum size ℓ around a point $\boldsymbol{x}$ (which is located in the plane of measurement), and $\mathcal{S}_\ell(\boldsymbol{x})$ the subset of $\mathcal{B}_\ell(\boldsymbol{x})$ of velocity increments with zero component in the direction perpendicular to the plane of measurement. Let us further denote S the area of $\mathcal{S}$, and V the volume of $\mathcal{V}$, and we define

$$\begin{aligned} \int_{\mathcal{S}} d\boldsymbol{r}\ |\boldsymbol{\nabla} G_\ell(\boldsymbol{r})| &= \frac{C_G}{\ell}, \\ \int_{\mathcal{V}} d\boldsymbol{r}\ |\boldsymbol{\nabla} G_\ell(\boldsymbol{r})| &= \frac{D_G}{\ell}, \end{aligned} \tag{32}$$

we have from Cauchy-Schwarz inequality

$$\begin{aligned} |\Pi^{\ell,2D}_{DR}(\boldsymbol{u})| &\leq \int_{\mathcal{S}} d\boldsymbol{r}\ |\boldsymbol{\nabla} G_\ell(\boldsymbol{r})| \int_{\mathcal{S}} d\boldsymbol{r}\ |\delta^{2D}\boldsymbol{u}(\boldsymbol{r})|^3, \\ &\leq \frac{C_G}{\ell} \left(\sup_{\mathcal{S}_\ell} |\delta^{2D}\boldsymbol{u}(\boldsymbol{r})| \right)^3 S, \\ &\leq \frac{C_G}{\ell} \left(\delta u(\boldsymbol{x},\ell)\right)^3 S, \end{aligned} \tag{33}$$

with $\delta u(\boldsymbol{x},\ell) = \sup_{\mathcal{B}_\ell} |\delta\boldsymbol{u}(\boldsymbol{r})|$ (see Sec. II A). On the other hand, we have also

$$\begin{aligned} |\Pi^{\ell}_{DR}| &\leq \int_{\mathcal{V}} d\boldsymbol{r}\ |\boldsymbol{\nabla} G_\ell(\boldsymbol{r})| \int_{\mathcal{V}} d\boldsymbol{r}\ |\delta\boldsymbol{u}(\boldsymbol{r})|^3, \\ &\leq \frac{D_G}{\ell} \left(\delta u(\boldsymbol{x},\ell)\right)^3 V. \end{aligned} \tag{34}$$

Now, if $\delta u(\boldsymbol{x},\ell) \sim \ell^h$ as $\ell \to 0$, then $\left(\sup_{\mathcal{V}_\ell} |\delta\boldsymbol{u}(\boldsymbol{r})|\right)^3 = O\left(\ell^{3h}\right)$, so that both SPIV and TPIV estimates decay to zero for $h > 1/3$. Therefore, the detection of dissipative Euler quasi-singularities via extreme events of $|\Pi^{\ell,2D}_{DR}(\boldsymbol{u})|$ does

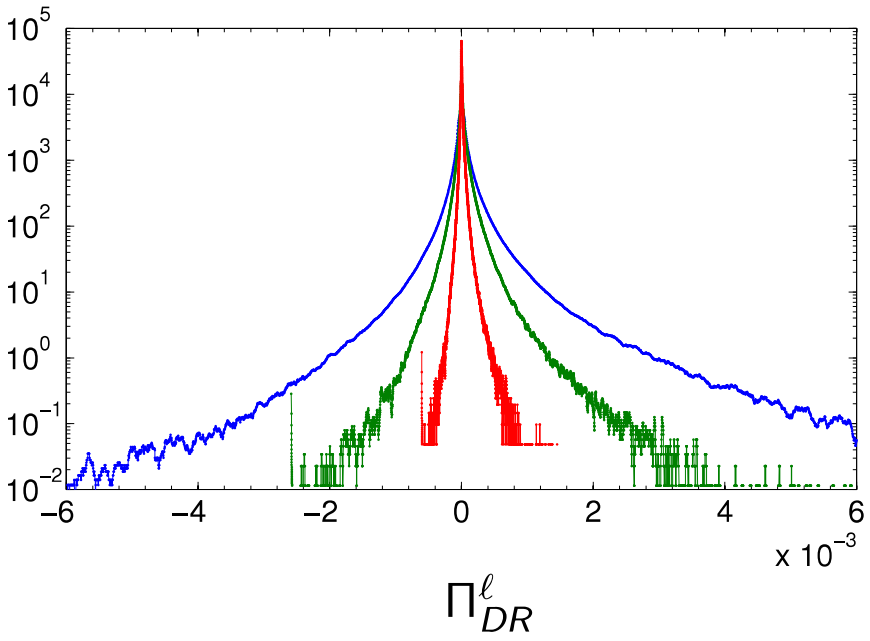

FIG. 3: Spacetime probability density distribution of the Duchon-Robert (DR) transfers Π^{ℓ}_{DR} at the three different scales studied on Fig. 2(a). The blue curve represents the smallest scale, and the red one the largest.

not introduce any spurious structures which would disappear when performing the full 3D computation. However, we cannot detect maxima corresponding to increments lying only on the y-direction from SPIV data. It is then sufficient to use the criterion based on $\Pi^{\ell,2D}_{DR}$, but it is not a necessary condition.
An illustration of this result can be provided by an application to our experimental data. In such a case, there is a strong streamwise mean flow and singularities are more likely to occur in the direction orthogonal to this plane. We thus choose y as the streamwise direction and compare the DR criterion applied on SPIV and TPIV data via instantaneous maps of $\Pi^{\ell,2D}_{DR}(\boldsymbol{u})$ (Fig. 4(a)) and $\Pi^{\ell}_{DR}(\boldsymbol{u})$ (Fig. 4(b)) obtained from the same data as in Fig. 6. Even though there are some differences between the two maps, it can be seen that both fields are qualitatively the same. This confirms that all areas where $\Pi^{\ell,2D}_{DR}(\boldsymbol{u}) \neq 0$ are also areas where $\Pi^{\ell}_{DR}(\boldsymbol{u}) \neq 0$. In order to quantify the correlation between both maps, we have performed the computation of the Pearson's coefficient R of linear correlation between areas of high energy transfer in $\Pi^{\ell,2D}_{DR}(\boldsymbol{u})$ and in $\Pi^{\ell}_{DR}(\boldsymbol{u})$. We find $R = 0.96$, where the threshold of $Q = 3$ has been used to define extreme events. The two fields are very well correlated, as expected.
Fig. 5 displays two planar cuts at z constant (a) and x constant (b), as represented on Fig. 4b). As described in [26], the velocity field is only available in a few planes along the streamwise direction. Here, we have only access to five of them. Therefore, the resolution of the flow is not as good along the y direction as it is for x and z. However, we can see that at the resolution of our PIV system, the structures we observe appear to be three-dimensional.

D. Complementary study : Comparison with vorticity

For vanishing viscosity, the Euler equations govern the dynamics of a fluid. In this case, it has been shown [51] that if $\boldsymbol{u}$ is a regular solution up to some blowup time T_*, then the vorticity $\boldsymbol{\omega}(\boldsymbol{x}, t)$ satisfies

$$\int_0^{T_*} ||\boldsymbol{\omega}(\boldsymbol{x}, t)||_\infty dt = \infty. \tag{35}$$

Therefore, a necessary and sufficient condition for the existence of a finite-time singularity is the blow-up of vorticity at T_*. This criterion (hereafter referred to as Beale-Kato-Majda (BKM) criterion) is usually used in numerical detection

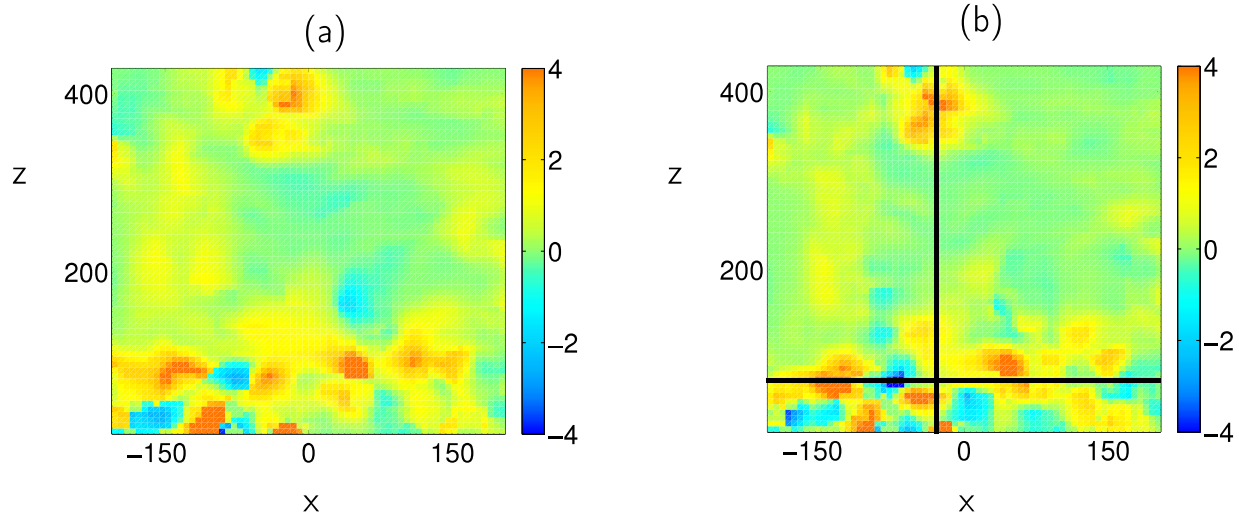

FIG. 4: Comparison between two instantaneous maps of the Duchon-Robert (DR) criterion computed from both SPIV and TPIV data. (a) map of the DR energy transfers $\Pi_{DR}^{\ell,2D}$ and (b) map of the DR energy transfers Π_{DR}^{ℓ} (normalized by their standard deviations). The results are displayed in the plane $y = 0$ orthogonal to the streamwise direction for the same data as in Fig. 2. The two orthogonal lines on map (b) represent the two planar cuts displayed on Fig. 5.

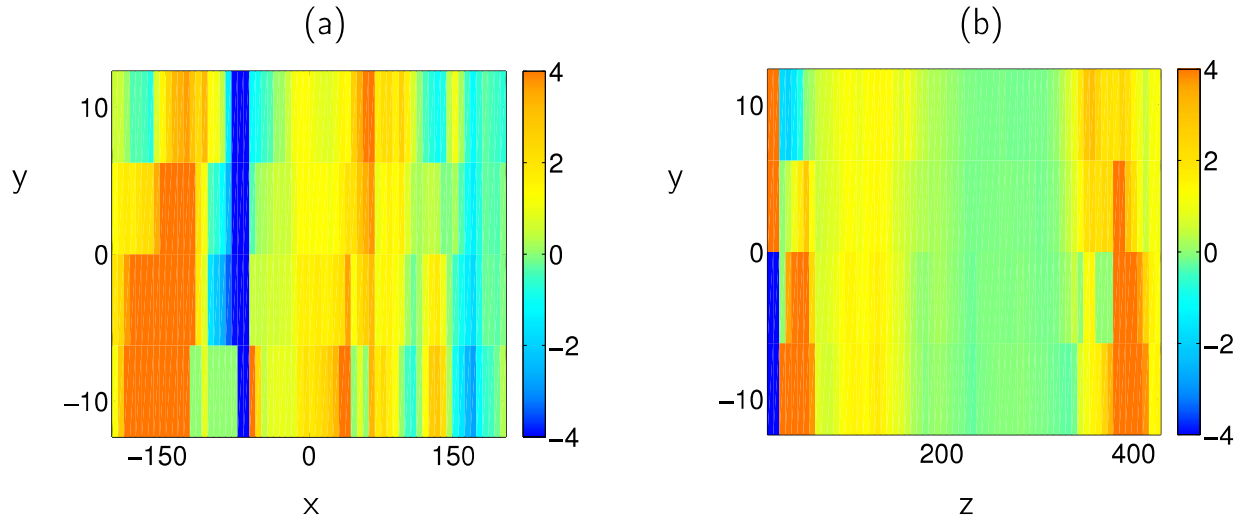

FIG. 5: Instantaneous maps of the Duchon-Robert (DR) energy transfers, in the two planes represented by black lines on Fig. 4, normalized by their space-time averages. (a) shows a planar cut in an (XY) plane and (b) shows a planar cut in a (ZY) plane for the same data as in Fig. 2. These maps allow us to see that the structures we detect appear to have a three dimensional structure.

of singularities in Euler equations. For finite viscosity, the regularity of the solutions to the INSE is controlled by putting an upper bound on the norm of the velocity field [9–11]. Therefore, Navier-Stokes singularities require the blow-up of the velocity field, and thus of the vorticity.

In order to make the discussion a little more precise, let us introduce the Sobolev spaces $H^s\left(\mathbb{R}^3\right)$, which consist of square-integrable functions whose distributional derivatives up to order s are also square-integrable, s being a positive integer. The associated norm on these spaces is denoted $||\cdot||_{H^s}$. Let us now assume that the hypothesis of the BKM theorem are true, *i.e.* for all $t \in [0, T_*[\,, \boldsymbol{u}\left(t\right) \in H^s\left(\mathbb{R}^3\right)$ for some $s \geqslant 3$. It can be shown from the Sobolev embedding theorem (see [52]) that before the blow-up occurs, $\boldsymbol{u}\left(t\right)$ is necessarily Hölder continuous for $0 < h \leqslant 1/2$. This rules

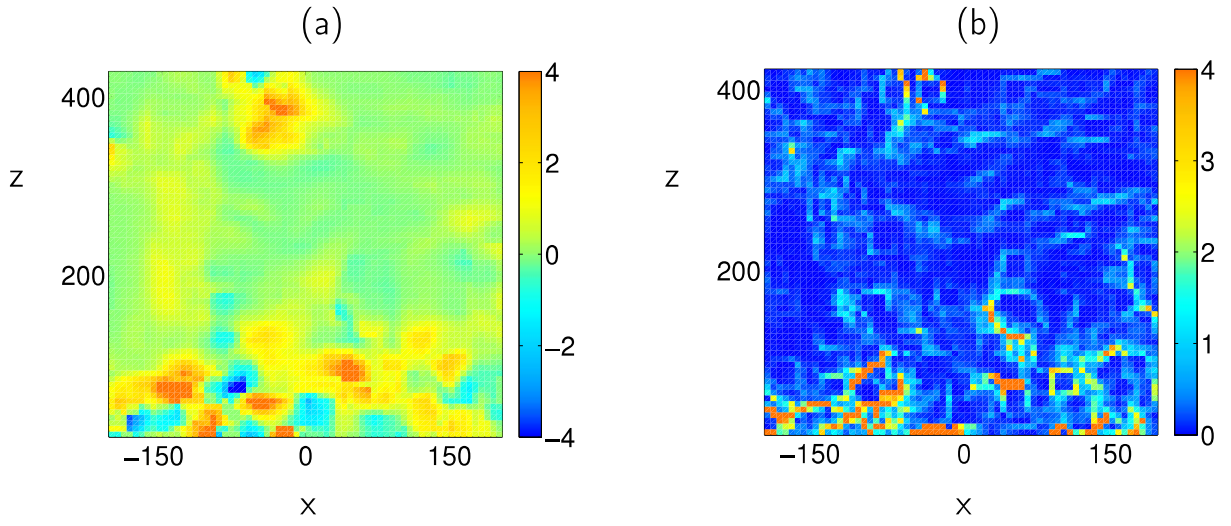

FIG. 6: Comparison between the Duchon-Robert (DR) criterion and the vorticity field using TPIV data. (a) map of the DR energy transfers Π^ℓ_{DR} and (b) map of the norm of the vorticity $|\boldsymbol{\omega}(x,z)|$ (normalized by their standard deviation). The results are displayed in the plane $y = 0$ orthogonal to the streamwise direction for the same data as in Fig. 2.

out Onsager's scenario up to T_*. In other words, a necessary condition for dissipative singularities to occur is the blow-up of $||\boldsymbol{u}||_{H^s}$, which is just what happens as T_* is approached since the vorticity becomes unbounded. As a consequence, it makes sense to compare the results obtained from the DR criterion with the vorticity field. Let us look at Fig. 6, where maps of $\Pi^\ell_{DR}(\boldsymbol{u})$ and $|\boldsymbol{\omega}(x,z)|$ (both normalized by their standard deviation) are displayed.
First of all, we observe on Fig. 6(b) that the vorticity is almost zero everywhere, except for some areas where it is concentrated into thin filaments of high intensity. Moreover, comparing Fig. 6(a) with Fig. 6(b), it can be seen that areas where the structures of dissipation detected by the DR criterion are localized are also areas where the norm of the vorticity is high. In order to quantify how much both maps are related, we compute the Pearson's coefficient R_N of linear correlation between areas where both criteria show intense events. We find $R_N = 0.84$, where the threshold of $Q = 3$ has been used to define extreme events. Therefore, we observe that areas of strong energy transfers in $\Pi^\ell_{DR}(\boldsymbol{u})$ are well correlated with areas of strong vorticity.
Let us now investigate whether there still is a high correlation between the DR criterion and the vorticity field when using SPIV data. The maps are displayed on Fig. 7. In the case of SPIV data, the only component of the vorticity that we are able to reconstruct is the one orthogonal to the plane of measurement (here ω_y). Therefore, the question we ask is: does the link between the BKM and DR criteria still exist when using SPIV data? Or put another way, are areas of strong DR energy transfer also areas where ω_y is high? Comparing both maps on Fig. 7, there indeed seems to be a correlation between both maps. We can quantify this correlation by once again computing the correlation coefficient $R_y = 0.75$. As a consequence, the relation between the DR and BKM criteria seems to hold well for this geometry, whether for TPIV or for SPIV data. However, there is no guarantee that it is still the same in other geometries.

IV. SINGULARITY DETECTION THROUGH EYINK FORMULA

A few years after the publication of [20], Eyink noticed that singularities may also cause a breakdown of Kelvin's theorem [21–23], in the sense that in addition to a nonzero energy dissipation rate, they might also produce a nonzero rate of velocity circulation decay $\Gamma_\ell(\boldsymbol{u})$ given by

$$\frac{d}{dt}\Gamma_\ell(\boldsymbol{u}) = \oint_{\mathscr{C}} d\boldsymbol{s}\cdot\mathscr{F}_{\boldsymbol{\ell}}(\boldsymbol{u}), \tag{36}$$

where

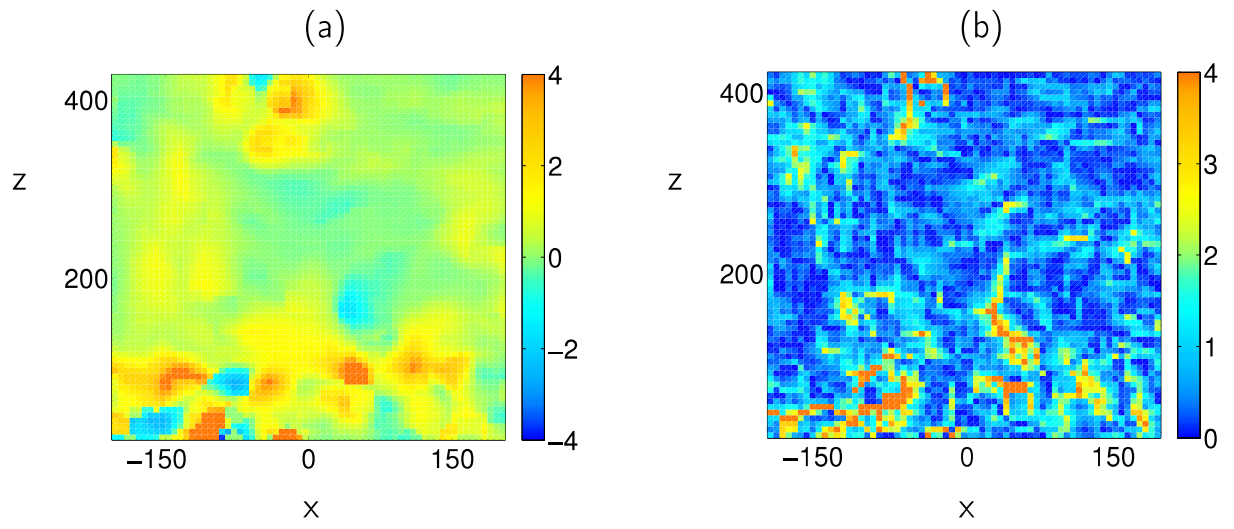

FIG. 7: Comparison between the Duchon-Robert (DR) criterion and the vorticity field using SPIV data. (a) map of the 2D DR energy transfers $\Pi_{DR}^{\ell,2D}$ and (b) map of the absolute value of the y-component of the vorticity $|\omega_y(x,z)|$ (normalized by their standard deviation) at the smallest resolved scale. The results are displayed in the plane $y = 0$ orthogonal to the streamwise direction for the same data as in Fig. 6.

$$\mathscr{F}_{\boldsymbol{\ell}}(\boldsymbol{u}) = \frac{1}{\ell}\int_{\mathcal{V}} d\boldsymbol{r}\ \left[\left(\delta\boldsymbol{u}(\boldsymbol{r}) - \int_{\mathcal{V}} d\boldsymbol{r}' G_\ell(\boldsymbol{r}')\delta\boldsymbol{u}(\boldsymbol{r}')\right)\cdot\boldsymbol{\nabla}G_\ell(\boldsymbol{r})\right]\ \delta\boldsymbol{u}(\boldsymbol{r}). \tag{37}$$

and $\mathscr{C}$ is a contour advected by the fluid. $\mathscr{F}_{\boldsymbol{\ell}}(\boldsymbol{u})$ is called the turbulent vortex-force. This is an important remark since Kelvin's theorem plays an important role in Taylor's vortex stretching mechanism for energy dissipation [18, 19, 23].

A. Detection method

We have seen in Sec. II and III that the velocity field $\boldsymbol{u}$ of a flow might develop singularities due to some internal mechanisms in the INSE, which are not fully understood. At the points in spacetime where this happens, $\boldsymbol{u}$ might however satisfy some Hölder continuity property with exponent h. At points where $h > 1/3$, no additional dissipation to viscosity occurs according to Onsager's arguments. However, if $h \leqslant 1/3$ an additional energy dissipation (or production) might appear [20, 23] causing kinetic energy to cascade through scales. Our detection method introduced in Sec. III is based on the computation of this additional term to the energy balance at scale ℓ and then track areas where it does not vanish with decreasing scale.

We introduce now a very similar detection method which is based on the observation that the turbulent vortex-force in (37) satisfies $\mathscr{F}_\ell(\boldsymbol{u}) = O(\delta u(\ell)^2/\ell) = O(\ell^{2h-1})$ if $\delta u(\ell) \sim \ell^h$ in the small scale limit, as discussed in [21–23]. Therefore, the computation of the turbulent vortex-force allows us to track dissipative Euler-quasi singularities or Navier-Stokes singularities with $h \leqslant 1/2$, whereas the DR criterion only allows us to track the ones with $h \leqslant 1/3$. Moreover, just as for the DR term, this computation only involves velocity increments, which are easily accessible via PIV measurements. For the same reason mentioned in Sec. III A, a detection criterion based on circulation production is only a necessary but not sufficient one (since our PIV set-up is not space resolved). Keeping the same test function G as in Eq. (30), we can implement a detection method very similar to the one described in Sec. III, but based on another cascading quantity. Therefore, two questions arise. Starting from our TPIV data and computing maps of $\mathscr{D}_\ell(\boldsymbol{u})$ and $\frac{d}{dt}\Gamma_\ell(\boldsymbol{u})$, are intense events in both cases well correlated? Are we able to detect areas where a strong circulation production is observed while the DR term is weak? This could mean the detection of non-dissipative Euler quasi singularities with $1/3 < h \leqslant 1/2$.

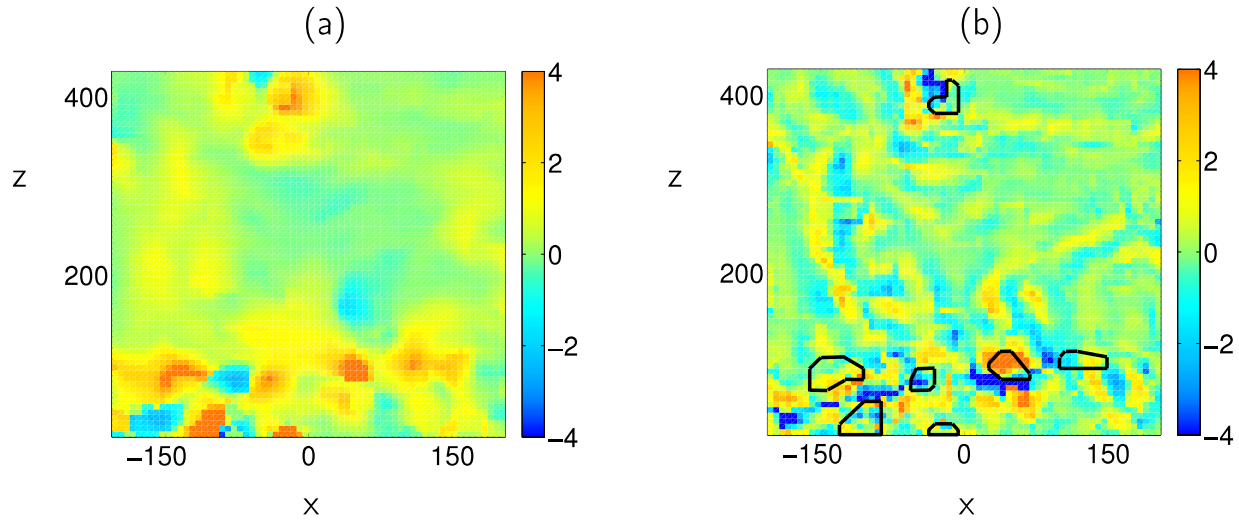

FIG. 8: Comparison between energy transfers and rate of circulation decay using SPIV data. (a) map of the DR energy transfers Π^ℓ_{DR} and (b) map of the rate of circulation decay $\frac{d}{dt}\Gamma_\ell(\boldsymbol{u})$ (normalized by their standard deviation). The results are displayed in the plane $y = 0$ orthogonal to the streamwise direction, and for the same data as in Fig. 2. For easier comparison, we have reported on the circulation map the contours of the areas where the DR dissipation is larger than three times its standard deviation. We observe intense events in both maps.

B. Implementation of the method

The arguments which have been made in Sec. III C to show that it is enough to look for quasi-singularities from SPIV via energy transfers can be once again made here. Therefore, in the following, we will focus on SPIV data.
Let us first compare maps of $\Pi^\ell_{DR}(\boldsymbol{u})$ (we drop the superscript "2D") and $\frac{d}{dt}\Gamma_\ell(\boldsymbol{u})$ in order to answer the first question. On Fig. 8 are displayed maps of these two quantities (normalized by their standard deviation) for the same data set as in Fig. 4(a).
First of all, it can be observed that areas where $\frac{d}{dt}\Gamma_\ell(\boldsymbol{u})$ is nonzero are organized as very thin filaments. In addition, Fig. 8(b) is more noisy than Fig. 8(a) even though the same procedure is applied in both cases, i.e. a derivative in scale is applied on the smoothing function, followed by a local angle averaging. There appears to be some correlation between the maps: in areas where Π^ℓ_{DR} is strong, there always is some nonzero circulation decay. However, we observe that regions of largest rate of circulation decay are either shifted with respect to areas of strong dissipation, or exist in some areas where there is little energy transfers (see contours on Fig. 8(b)). Overall, the Pearson's coefficient of linear correlation R_Γ between regions of strong events ($Q = 3$) in both fields is $R_\Gamma = 0.85$. We therefore obtain a good correlation between areas where both $\frac{d}{dt}\Gamma_\ell(\boldsymbol{u})$ and Π^ℓ_{DR} are strong, which is consistent with the possibility that Euler singularities may cause a break-down of Kelvin's theorem.
Fig. 9 displays the spacetime probability distribution of $d\Gamma_\ell/dt$ in the same XZ-plane studied up to now, in the stationary regime. Here again, we observe a strongly non-Gaussian statistics with very wide tails, which confirms that $d\Gamma_\ell/dt$ can be used a criterion to detect possible singularities through scales. However, the fact that the maps of circulation are more noisy than the maps of dissipation renders their use less straightforward to detect quasi-singularities.

V. DISCUSSION

In this paper, we have introduced two new methods based on the work of Duchon, Robert and Eyink [20–23], which allow for the local detection of dissipative Euler quasi-singularities or Navier-Stokes singularities in experimental flows. Both criteria assume the knowledge of spatial velocity increments only and are therefore easy to implement experimentally as well as numerically. The key idea behind their implementation is that velocity field in turbulent flows might lose some regularity while satisfying Hölder continuity conditions with an exponent $h \leqslant 1$ in the limit of small scales. If $h \leqslant 1/2$, a cascade of circulation might occur and Kelvin theorem breaks down. This cascade can

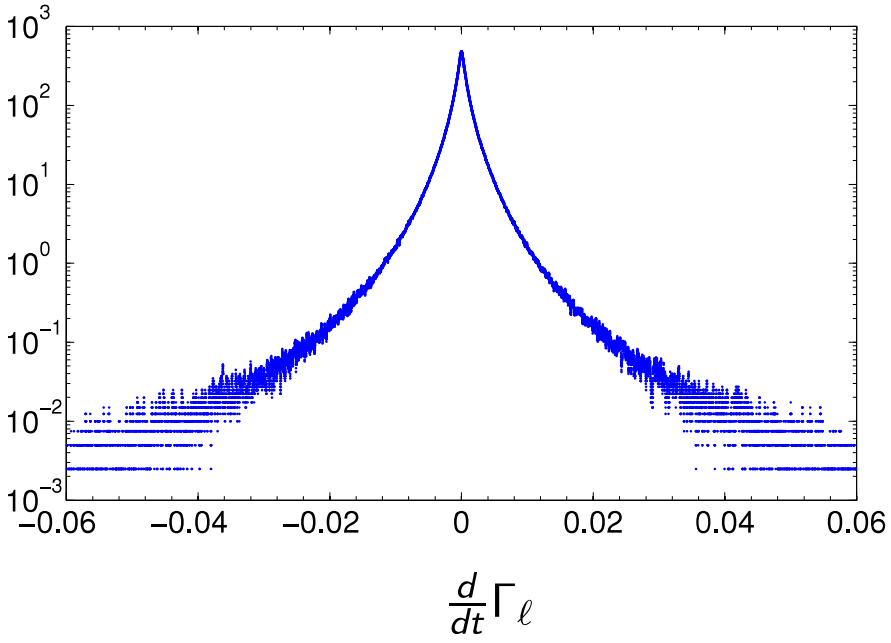

FIG. 9: Spacetime probability density distribution of the velocity circulation decay $d\Gamma_\ell/dt$.

be detected at larger scales provided that we are in the inertial range. In the same way, if $h \leqslant 1/3$, then a cascade of energy might occur which can also be detected in the inertial range. The first criterion that we introduced (DR criterion) focuses on these energy transfers, which are described by Π^ℓ_{DR} (see Eq. 7).

From its probability distribution, we observed in Sec. III B that Π^ℓ_{DR} has a strongly non-Gaussian statistics, with very wide tails, in agreement with [50]. This indicates the existence of extreme events which might correspond to Euler quasi-singularity or genuine Navier-Stokes singularities. In addition, we saw that as the scale is decreased, the standard deviation of Π^ℓ_{DR} increases, which results in the tails of the distribution getting wider.

Furthermore, since Navier-Stokes singularities concern the blow-up of the velocity field, we expect to observe a very strong vorticity at the location of possible singularities. As a consequence, we compared the DR criterion with the vorticity field, and found a good agreement between them, whether SPIV or TPIV data sets are considered.

We also showed analytically that to detect singularities, one does not need to have access to the whole velocity field inside a volume, but can instead look for them from stereoscopic particle image velocimetry (SPIV) data on a plane. This is confirmed by performing both 2D and 3D computations and comparing maps of the DR term $\Pi^\ell_{DR}(\boldsymbol{u})$ from TPIV measurements obtained inside the boundary layer of a wind tunnel [26]. Clearly, being limited to SPIV data means the informations along a third direction are lacking meaning that quasi-singularities with structure in the third direction cannot be detected. In this flow, we observe that the computation of the DR term actually shows areas where it is nonzero, some of them being characterized by very strong (extreme) energy transfers through scales.

Finally, we investigated a second new method for the detection of singularities based on the possibility of a breakdown of Kelvin theorem at very large Reynolds numbers [21–23]. We showed that this method is well correlated with the DR criterion even though areas of intense energy transfers are sometimes shifted compared to areas of high rate of circulation. However, due to higher noise, this method is less reliable than the DR method, but it may allow for the detection of a wider range of singularities.

In the present paper, our detection methods were applied inside a boundary layer geometry, the resolution of our data being close to, but not exactly reaching, the dissipative scale. The fact that we detect areas with negative Π^ℓ_{DR} suggests that we observe energy transfers through scales [30], but not dissipation due to singularities. This is a strong indication that the Kolmogorov scale η is not the smallest relevant scale for energy dissipation and that there might actually exist smaller scales at which dissipation takes place, as suggested in the multifractal picture of turbulence. To get stronger conclusions about the existence and topology of dissipative Euler quasi singularities or Navier-Stokes singularities in experimental flows, we need measurements with a resolution smaller than the Kolmogorov scale. An attempt in that direction is made in [50] . We hope our work will help providing experimental constraints on the

properties of Navier-Stokes singularities as well as on corresponding suitable weak solutions.

Acknowledgements

E.-W. Saw acknowledges support from the EuHIT contract FP7-INFRASTRUCTURE Collaborative Project no: 312778. D. Faranda's work was supported by CNRS during his post-doc.

[1] J.L. Lions and G. Prodi. Un théorème d'existence et d'unicité dans les équations de navier-stokes en dimension 2. *Comptes rendus de l'Académie des Sciences*, 248:3519–3521, 1959.

[2] J.L. Lions. *Quelques Méthodes de Résolution des Problèmes aux Limites Non Linéaires*. 1969.

[3] O. A. Ladyzhenskaya. *The Mathematical Theory of Viscous Incompressible Flow*, volume 2 of *Mathematics and Its Applications*. Gordon and Breach, second edition, 1969.

[4] Y. Giga. Weak and strong solutions of the navier-stokes initial value problem. *Publications of the Research Institute for Mathematical Sciences*, 19:887–910, 1983.

[5] C.L. Fefferman. Existence and smoothness of the navier-stokes equation. The Millennium Prize Problems, 2006.

[6] J. Leray. Etude de diverses équations intégrales nonlinéaires et de quelques problèmes que pose l'hydrodynamique. *Journal de Mathématiques Pures et Appliquées*, 12(9):1–82, 1933.

[7] J. Leray. Sur le mouvement d'un liquide visqueux emplissant l'espace. *Acta Mathematica*, 63(1):193–248, July 1934.

[8] J. Leray. Essai sur les mouvements plans d'un liquide visqueux que limitent des parois. *Journal de Mathématiques Pures et Appliquées*, 13(9):331–418, 1934.

[9] J. Serrin. On the interior regularity of weak solutions of the Navier-Stokes equations. *Archive for Rational Mechanics and Analysis*, 9:187–195, January 1962.

[10] L. Escauriaza, G.A. Seregin, and V. Sverak. $l_{3,\infty}$ -solutions of the navier-stokes equations and backward uniqueness. *Russian Mathematical Surveys*, 58(2):211, 2003.

[11] P. Constantin. Euler and navier-stokes equations. *Publicacions Matemàtiques*, 52(2):235–265, 2008.

[12] U. Frisch. *Turbulence*. Cambridge University Press, 1995.

[13] P. Constantin and C. Fefferman. Scaling exponents in fluid turbulence: some analytic results. *Nonlinearity*, 7:41–57, January 1994.

[14] P. Constantin. Geometric statistics in turbulence. *SIAM Review*, 36(1):73–98, 1994.

[15] L. Caffarelli, R. Kohn, and L. Nirenberg. Partial regularity of suitable weak solutions of the Navier-Stokes equations. *Communications in Pure Applied Mathematics*, 35:771–831, November 1982.

[16] G. L. Eyink and K. R. Sreenivasan. Onsager and the theory of hydrodynamic turbulence. *Reviews of Modern Physics*, 78:87–135, January 2006.

[17] L. Onsager. Statistical hydrodynamics. *Nuovo Cimento (Suppl.)*, 6:279–287, 1949.

[18] G. I. Taylor and A. E. Green. Mechanism of the Production of Small Eddies from Large Ones. *Proceedings of the Royal Society of London Series A*, 158:499–521, February 1937.

[19] G. I. Taylor. Production and Dissipation of Vorticity in a Turbulent Fluid. *Proceedings of the Royal Society of London Series A*, 164:15–23, January 1938.

[20] J. Duchon and R. Robert. Inertial energy dissipation for weak solutions of incompressible Euler and Navier-Stokes equations. *Nonlinearity*, 13:249–255, January 2000.

[21] S. Chen, G. L. Eyink, M. Wan, and Z. Xiao. Is the Kelvin Theorem Valid for High Reynolds Number Turbulence? *Physical Review Letters*, 97(14):144505, October 2006.

[22] G. L. Eyink and H. Aluie. The Cascade of Circulations in Fluid Turbulence. In *APS Division of Fluid Dynamics Meeting Abstracts*, November 2006.

[23] G. L. Eyink. Dissipative anomalies in singular Euler flows. *Physica D Nonlinear Phenomena*, 237:1956–1968, August 2008.

[24] J. F. Muzy, E. Bacry, and A. Arneodo. Wavelets and multifractal formalism for singular signals: Application to turbulence data. *Physical Review Letters*, 67:3515–3518, 1991.

[25] P. Kestener and A. Arneodo. Generalizing the Wavelet-Based Multifractal Formalism to Random Vector Fields: Application to Three-Dimensional Turbulence Velocity and Vorticity Data. *Physical Review Letters*, 93(4):044501, July 2004.

[26] F.J.W.A. Martins, J.-M. Foucaut, L. Thomas, L.F.A. Azevedo, and M. Stanislas. Volume reconstruction optimization for tomo-piv algorithms applied to experimental data. *Measurement Science and Technology*, 26, 2015.

[27] P. Constantin, E. Weinan, and E. S. Titi. Onsager's conjecture on the energy conservation for solutions of Euler's equation. *Communications in Mathematical Physics*, 165:207–209, October 1994.

[28] G. L. Eyink. Energy dissipation without viscosity in ideal hydrodynamics I. Fourier analysis and local energy transfer. *Physica D Nonlinear Phenomena*, 78:222–240, November 1994.

[29] B. Dubrulle. A weak formulation of the kármán-howarth equation. Submitted to EPL.

[30] D. Kuzzay, D. Faranda, and B. Dubrulle. Global vs local energy dissipation: The energy cycle of the turbulent von Kármán flow. *Physics of Fluids*, 27(7):075105, July 2015.

[31] G. I. Taylor. Statistical Theory of Turbulence. *Royal Society of London Proceedings Series A*, 151:421–444, September 1935.

[32] G. Comte-Bellot and S. Corrsin. Simple Eulerian time correlation of full- and narrow-band velocity signals in grid-generated, 'isotropic' turbulence. *Journal of Fluid Mechanics*, 48:273–337, 1971.

[33] R. M. Williams and C. A. Paulson. Microscale temperature and velocity spectra in the atmospheric boundary layer. *Journal of Fluid Mechanics*, 83:547–567, December 1977.

[34] D. P. Lathrop, J. Fineberg, and H. L. Swinney. Transition to shear-driven turbulence in Couette-Taylor flow. *Physical Review A*, 46:6390–6405, November 1992.

[35] O. Cadot, Y. Couder, A. Daerr, S. Douady, and A. Tsinober. Energy injection in closed turbulent flows: Stirring through boundary layers versus inertial stirring. *Physical Review E*, 56:427–433, July 1997.

[36] J. Jimenez, A. A. Wray, P. G. Saffman, and R. S. Rogallo. The structure of intense vorticity in isotropic turbulence. *Journal of Fluid Mechanics*, 255:65–90, 1993.
[37] L.-P. Wang, C. Shiyi, J.G. Brasseur, and J.C. Wyngaard. Examination of hypotheses in the kolmogorov refined turbulence theory through high-resolution simulations. part 1. velocity field. *Journal of Fluid Mechanics*, 309:113–156, 1996.
[38] P. K. Yeung and Y. Zhou. Universality of the Kolmogorov constant in numerical simulations of turbulence. *Physical Review E*, 56:1746–1752, August 1997.
[39] N. Cao, S. Chen, and G. D. Doolen. Statistics and structures of pressure in isotropic turbulence. *Physics of Fluids*, 11:2235–2250, August 1999.
[40] T. Gotoh, D. Fukayama, and T. Nakano. Velocity field statistics in homogeneous steady turbulence obtained using a high-resolution direct numerical simulation. *Physics of Fluids*, 14:1065–1081, March 2002.
[41] Y. Kaneda, T. Ishihara, M. Yokokawa, K. Itakura, and A. Uno. Energy dissipation rate and energy spectrum in high resolution direct numerical simulations of turbulence in a periodic box. *Physics of Fluids*, 15:L21–L24, February 2003.
[42] A. N. Kolmogorov. The local structure of turbulence in incompressible viscous fluid for very large reynolds number. *Akademiia Nauk SSSR Doklady*, 30:9–13, 1941.
[43] T. de Karman and L. Howarth. On the Statistical Theory of Isotropic Turbulence. *Proceedings of the Royal Society of London Series A*, 164:192–215, January 1938.
[44] A. S. Monin. The Theory of Locally Isotropic Turbulence. *Soviet Physics Doklady*, 4:271, October 1959.
[45] A. S. Monin and A. M. Yaglom. *Statistical Fluid Mechanics*, volume 2. J. Lumley, MIT Press, Cambridge, MA, 1975.
[46] G. L. Eyink. Lecture notes on turbulence.
[47] G. Parisi and U. Frisch. On the singularity structure of fully developed turbulence. In M. Ghil, R. Benzi, and G. Parisi, editors, *Turbulence and Predictability in Geophysical Fluid Dynamics*, pages 84–87, 1985.
[48] G. Paladin and A. Vulpiani. Anomalous scaling and generalized Lyapunov exponents of the one-dimensional Anderson model. *Physical Review B*, 35:2015–2020, February 1987.
[49] V. et al. Lucarini. *Extremes and Recurrence in Dynamical Systems*. Wiley, 2016.
[50] E.-W. Saw, D. Kuzzay, D. Faranda, A. Guittonneau, F. Daviaud, C. Wiertel-Gasquet, V. Padilla, and B. Dubrulle. Experimental characterization of extreme events of inertial dissipation in a turbulent swirling flow. *Nature Communications*, 7:12466, August 2016.
[51] J. T. Beale, T. Kato, and A. Majda. Remarks on the breakdown of smooth solutions for the 3- D Euler equations. *Communications in Mathematical Physics*, 94:61–66, March 1984.
[52] R.A. Adams. *Sobolev Spaces*. Academic Press, Inc., 1975.